NDT&E International 86 (2017) 7–13

Contents lists available at ScienceDirect

NDT&E International

journal homepage: www.elsevier.com/locate/ndteint

Automated detection of welding defects in pipelines from radiographic images DWDI

Neury Boaretto[a,b,*], Tania Mezzadri Centeno[a]

[a] Program on Electrical Engineering and Computer Science (CPGEI), Federal University of Technology of Paraná (UTFPR), Av. Sete de Setembro, 3165, Rebouças, CEP 80230-901, Curitiba, PR, Brazil

[b] Department of Electronics, Federal Institute of Santa Catarina (IFSC), Rua Pavão, 1337, Costa e Silva, CEP 89220-200, Joinville, SC, Brazil

ARTICLE INFO

Keywords:
Pattern recognition
Non-destructive testing
Descontinuities classification
Artificial neural network
Welding defects detection

ABSTRACT

This paper presents a method for the automatic detection and classification of defects in radiographic images of welded joints obtained by exposure technique of double wall double image (DWDI). The proposed method locates the weld bead on the DWDI radiographic images, segments discontinuities (potential defects) in the detected weld bead and extracts features of these discontinuities. These features are used in a feed-forward multilayer perceptron (MLP) with backpropagation learning algorithm to classify descontinuities in "defect and no-defect". The classifier reached an accuracy of 88.6% and a F-score of 87.5% for the test data. A comparison of the results with the earlier studies using SWSI and DWSI radiographic images indicates that the proposed method is promising. This work contributes towards the improvement of the automatic detection of welding defects in DWDI radiographic image which results can be used by weld inspectors as a support in the preparation of technical reports.

1. Introduction

Non-destructive testing (NDT) are usually used for monitoring and ensuring the integrity of structures used in the oil and gas industry. Techniques of artificial intelligence and computer vision can be used to assist in interpreting the results of NDT and provide an estimate of diagnosis of the inspected material.

A variety of NDT are available for identification, and evaluation of defects in welded joints of pipes, being the ultrasound and radiography the most relevant. Radiographic methods are based on the partial absorption of penetrating radiation as it passes through the object under investigation. Radiographic testing is widely adopted in industry to non-destructively examine welded joints for possible flaws or defects in pipes and has significant advantages over other NDE techniques. In this technique, the analysis and interpretation are almost intuitive and it provides a permanent visible record of the volumetric inspection of material [1].

The human visual inspection of the radiograph requires an inspector who possesses extensive experience, visual accuracy and a full knowledge of the applied technique. The large number of images to be inspected causes an increase in the workload of the inspectors which can lead to a subjective interpretation with the potential risk of overlooking defects due to physical or mental fatigue [2].

For the reasons stated, there is a need for automatic tools able to efficiently assist inspectors in the detection of defects in welded joints. Computer vision and artificial intelligence techniques have been widely explored in research involving the analysis and interpretation of radiographs of welds through digital radiographic inspection. In this context many efforts have been made towards the design and construction of computers tools, aiming to support the weld joint radiographs interpretation and therefore improving robustness accuracy and speed of the inspection process. Therefore, various algorithms based on image processing, computer vision, artificial intelligence and other related fields were used to detect and classify welding defects from radiographic images. These algorithms include fuzzy reasoning [3], linear and nonlinear classifiers [4–10], texture analysis [11], expert systems [12], neural networks [13,14] and neuro-fuzzy inference [15].

All previously cited references use radiographic images acquired by Single Wall Single Image (SWSI) technique or Double Wall Single Image (DWSI) technique. In the literature, there is a lack of published research regarding Double Wall Double Image (DWDI) radiographic images.

DWDI exposure technique is a typical arrangement adopted for taking radiographic images of the pipe with a diameter equal to or less

* Corresponding author at: Program on Electrical Engineering and Computer Science (CPGEI), Federal University of Technology of Paraná (UTFPR), Av. Sete de Setembro, 3165, Rebouças, CEP 80230-901, Curitiba, PR, Brazil.
E-mail addresses: neury@ifsc.edu.br (N. Boaretto), mezzadri@utfpr.edu.br (T.M. Centeno).

http://dx.doi.org/10.1016/j.ndteint.2016.11.003
Received 24 February 2016; Received in revised form 7 November 2016; Accepted 9 November 2016
Available online 14 November 2016
0963-8695/

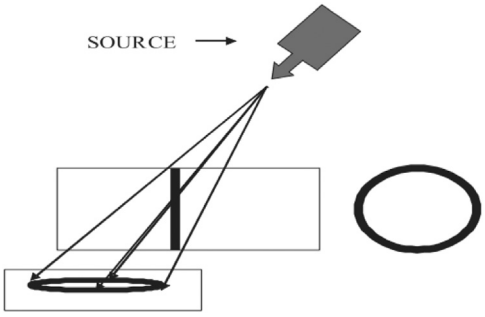

Fig. 1. DWDI radiographic testing.

than 90 mm thereby not allowing any internal access for the insertion of the radiation source. The source is positioned slightly far from the pipe, in such a way that the beam does not miss the nearest part of the weld. The source is kept at an inclination that avoids the overlapping of the top and bottom welds. Usually, two exposures are taken by rotating the pipe by 90 degrees. Thus, in DWDI we have radiographic images where both walls of a tubular section are superimposed, resulting in an elliptical image as shown in Fig. 1 [16]. At least two images of each welded joint are necessary for a complete weld bead inspection.

The optical density of a radiographic image is a function of the total number of photons reaching each point. The total number of photons results from the sum of the number of photons that cross the object and the number of scattered photons that cross the object after having interacting with the matter. The photons that pass through the object provide the image and the scattered photons result in increased image noise, blur and reduced image contrast. Therefore, scattered radiation reaching the film is an important cause of reducing image quality [17].

In the DWDI technique the radiation beam passes through both the walls of the pipe increasing the scattering. A research conducted by Edalati et al. [18] have been performed to measure the gamma ray or x-ray radiographic sensitivity for pipes and plates to compare the results with sensitivity requirements of the standards. Experiments revealed that the required sensitivity based on the single wall thickness was attainable for DWSI technique, but it could not be easily obtained for DWDI due to the high scattering. Therefore, the detection of low contrast defects in DWDI radiography of pipes is a challenging task for inspections [17].

The works [19–21] present techniques for weld bead detection in DWDI images but do not address the detection of detects in welded joints. In this context, as a contribution, this paper proposes an automated algorithm for detection and classification of defects in DWDI computerized radiographic images of welded joints in oil and gas pipelines. The experiments were performed on real field images which, usually, have a lower quality than the images used in other studies.

The paper is organized as follows: Section 2 describes the proposed method used for segmenting and classifying discontinuities in DWDI radiographic images of welds joints in pipes. The results obtained with real field images are presented in Section 3. Finally, Section 4 gives concluding remarks and suggestions for future research.

2. Materials and methods

Radiographic images can be acquired by several systems. Computed Radiography (CR) produces a digital image by using a Phosphor Imaging Plate (IP) in place of conventional film. This present study uses weld beads clipped from eight images obtained by Dürr Computed Radiography system. All the images are DWDI images in gray levels with 16 bits per pixel (bpp) of resolution and were inspected by experts. Such images have the most common types of defects in welded joints, such as porosity (PO), slag inclusion (SI), cracks (CR) and lack of fusion (LF). Fig. 2(b) shows the result of the inspection, conducted by an expert for the image in Fig. 2(a), where the defects slag inclusion (SI) and lack of fusion (LF) were detected.

2.1. Experimental procedure

Fig. 3 shows the main steps of the proposed algorithm for automatic detection and classification of defects in weld beads: location of the region of interest (ROI), detection of discontinuities (potential defects), extraction of features of the detected discontinuities and classification of the discontinuities.

2.1.1. Location of the weld bead region

The location of the weld bead region is performed on clippings of the original image, such as shown in Fig. 4(a) and aims to limit the search region for the next step (detection of discontinuities).

The segmentation of the weld bead is carried out through image processing techniques. Initially, in order to reduce the level of image noise a 9×9 median filter is applied on the clipping of the original image. Then a 300×300 average filter is applied on the resulting image generating a “blurring image”, as shown in Fig. 4(b). A constant value of 200 is added to the blurring image to increase the image brightness. Such an image is subtracted from the image filtered by the median filter, resulting in an unsharp mask. The adaptive thresholding described in [22] with threshold equal to 0 (zero) is applied to the mask, the result can be seen in Fig. 4(c). All values were determined empirically from experiments in order to reduce the search space and not exclude any discontinuity in the weld bead region.

In order to remove noises, regions with an area of less than 10.000 pixels are excluded. To prevent that discontinuities placed at the margin of the weld bead to be discarded, the resulting image is morphologically eroded with a disk structuring element of radius 23 pixels (size determined empirically), the result is shown in Fig. 4(d).

2.1.2. Detecting discontinuities and extraction of features

This step performs the detection of existing descontinuities in the ROI segmented in the previous step and extracts the features of the detected descontinuities to be subsequently used as inputs to a neural network in the classification step.

Radiographic images are commonly noisy as result of particular conditions in acquisition process. Noise, in this type of image, is generally characterized as randomly spread pixels, with intensity values different from their neighbouring pixels [15]. In order to reducing noise, an adaptive Wiener filter is used to estimate local gradient mean and standard deviation. The greater the standard deviation, the lower the smoothing performed by the filter and vice versa. The adaptive filter is more selective than a comparable linear filter, preserving edges and other high-frequency parts of an image.

So that, the adaptive filter Wiener 5×5 is applied to the clipping of the original image shown in Fig. 5(a). Next, to the filtered image is applied a top-hat operation [23], with a disk structuring element of radius 10 pixels. The resulting image is added to the clipping of original image to enhance small details highlighting the discontinuities. These operations showed no visible effects. Results can be viewed only after thresholding.

A blurring image is obtained by applying a 55×55 average filter on the resulting image. This image is added with a constant value of 40 and the result is subtracted from the image processed by the top-hat operation, resulting in an unsharp mask. A histogram equalization is applied to the mask to improve the brightness and contrast, whose result is shown in Fig. 5(c). This image is then thresholded by the Otsu method [24] resulting in the image shown in Fig. 5(d) which is added with the image of the ROI obtained in the previous step (Fig. 5(b)).

After performing the described operations, all objects with the area larger than 40 pixels and smaller than 6000 pixels are considered potential defects. Furthermore, all defects located within a range of 10% in the right and left ends of the image and 7% in the upper and

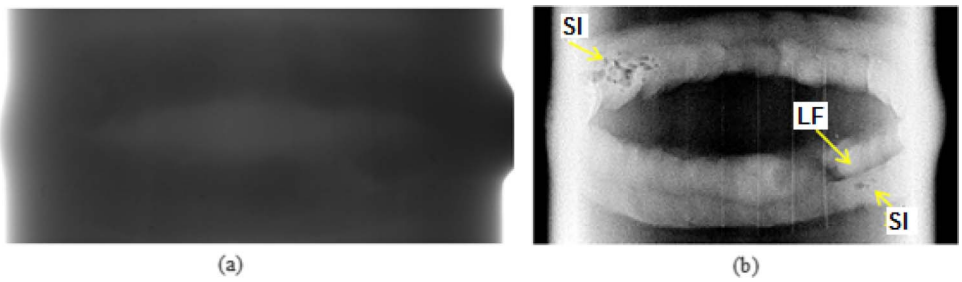

Fig. 2. (a) Clipping of the original image, (b) Report of inspection for the Fig. 2(a).

Fig. 3. Steps of the proposed algorithm for automatic detection and classification of defects in weld beads.

lower ends are discarded. This band is not part of the ROI, so discontinuities found in this region are excluded from the following steps. The results of this step and the previous step are shown in Fig. 5(e). The values used were defined empirically by comparing the segmented images and the inspected images.

The potential defects in Fig. 5(e) (white objects in the image) are identified using a labeling algorithm [25] and then their edges are obtained by morphological gradient [22,23]. Fig. 5(f) shows the discontinuities found and identified (potential defects).

After detecting the discontinuities, some relevant geometric features are extracted, that are fed as input to a neural network for classification. The following set of features are extracted for each detected discontinuity:

- Area (A): discontinuity area.
- Eccentricity (Ec): ratio of the distance between the foci of the ellipse that has the same second-moments as the region and its major axis length.
- Solidity (S): discontinuity area divided by the convex hull Area.
- Extension (Ex): ratio between the defect area and the area of the smallest rectangle surrounding the discontinuity.
- Ratio 1: ratio between the minor axis and the Area.
- Ratio 2: ratio between the major axis and the Area.
- Ratio 3: ratio between the major axis and the minor axis
- Rounding: Ratio $p^2/4\pi A$, where p is the perimeter and A is the discontinuity area.

From the descontinuities found in the eight images, we constructed a database of n feature vectors where each vector describes a discontinuity. Each vector contains 9 elements representing the 8 features and an element is allocated to identify the class corresponding to this vector.

2.1.3. Neural network training

After extracting the features from the descontinuities, the database is employed to train a neural network to classify the descontinuities in five classes (porosity, slag inclusion, lack of fusion, cracks and no defect). The network used is a feed-forward multilayer perceptron (MLP) with three layers. A block diagram of the proposed classifier is illustrated in Fig. 6. The network has eight inputs, (one for each feature), ten neurons in the hidden layer and five neurons in the output layer (one for each class). The activation functions at the hidden layer and output layer in the network are a hyperbolic tangent function, since it was the one that presented the best results for all the tests. The number of neurons in the hidden layer was chosen heuristically.

MLP is a feedforward artificial neural network model that maps sets of input data onto a set of appropriate output. Usually, MLP utilizes a supervised learning technique called backpropagation for training the network. MLP network with backpropagation learning algorithm is chosen due to its fast processing time and good performance for pattern recognition problems [26].

In order to learn, the network calculates the error, which is the difference between the desired response and the actual response, and a portion of it is propagated backwards through the network. At each neuron in the network the error is used to adjust weights, so that at the next epoch the error in the network response will be lower for the same inputs. This corrective procedure is called backpropagation and is applied continuously for each set of inputs or training data. Møller [27] introduced a scaled conjugate gradient method that instead of a line search uses an estimate of the second derivative along the search direction to find an approximation to

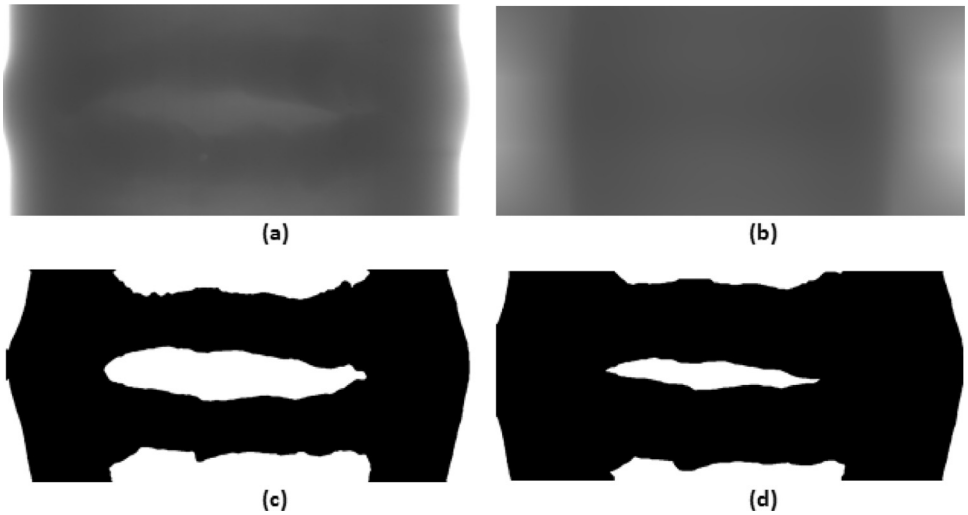

Fig. 4. Weld bead segmentation: (a) clipping of original image (b) result of average filter, (c) thresholded image and (d) eroded image.

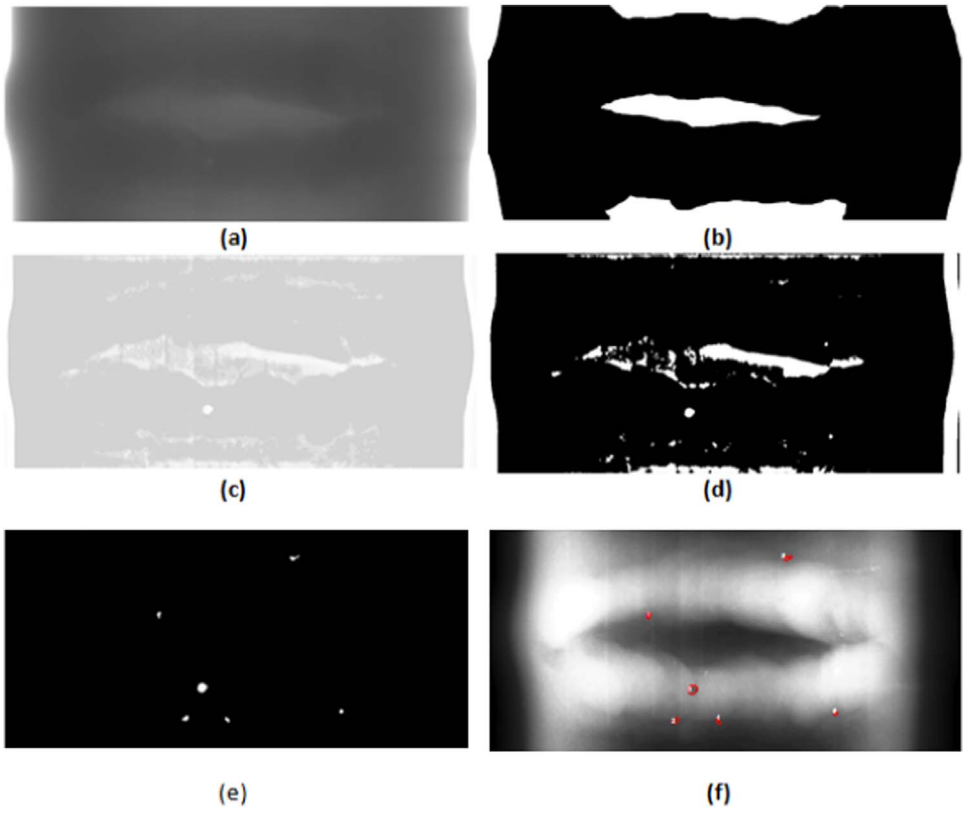

Fig. 5. Results of the main steps for detecting potential defects, (a) clipping of original image, (b) ROI, (c) equalized unsharp mask, (d) thresholded image, (e) detected discontinuities and (f) detection of potential defects.

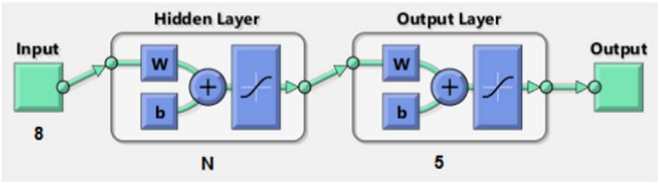

Fig. 6. MLP neural network with N neurons in the hidden layer.

the minimum error along the search direction.

In this approach, the scaled conjugated gradient technique was applied to find the best weights in the training process. In each training cycle, the input vectors are presented to the network. Neural network training continues until the change in error is not significant after six training cycles, this is the value used as a reference by Beale et al. [28].

The input vectors are partitioned into training, validation, and testing sub-sets, composed respectively by 70%, 15%, and 15% of the available samples, as suggested by Beale et al. [28].

2.1.4. Classifier performance measurement

Once a classifier is established, its performance can be evaluated by various methods. The efficiency of a classification can be evaluated by computing the number of correctly recognized class examples (true positives), the number of correctly recognized examples that do not belong to the class (true negatives), and examples that either were incorrectly assigned to the class (false positives) or that were not recognized as class examples (false negatives). These four counts constitute a confusion matrix shown in Fig. 7 for the case of the binary classification [29].

According to [30,31] using the confusion matrix, a set of statistical measures can be derived for the analytical evaluation, such as recall or sensitivity (true positive rate), precision and accuracy.

True positive rate (TPR) (recall or sensitivity): is the ratio of positives samples correctly classified to the actual number of positives

	True Condition		
Predicted condition	True Positive TP	False Positive FP	Precision
	False Negative FN	True Negative TN	
	Recall		Accuracy

Fig. 7. Sample confusion matrix of two classes.

samples (Eq. (1)).

$$\text{Recall}=TP/(TP+FN) \quad (1)$$

Accuracy: is the ratio of overall number of samples which are correctly classified to the total number of samples (Eq. (2)).

$$\text{Accuracy}=(TP+TN)/(TP+TN+FP+FN) \quad (2)$$

Precision: is the ratio of positives samples correctly classified to the number of samples classified as positive (Eq. (3)).

$$\text{Precision}=TP/(TP+FP) \quad (3)$$

Precision and recall are often combined into a single statistic called the F-score or F-measure which is the harmonic mean of precision and recall, defined in Eq. (4). F-score is fairly indicative of the performance of the overall algorithm.

$$F-\text{score} = 2\,x\,(\text{PrecisionxRecall})/(\text{Precision}+\text{Recall}) \quad (4)$$

3. Results and discussion

The input of the algorithm is the set of eight images described in

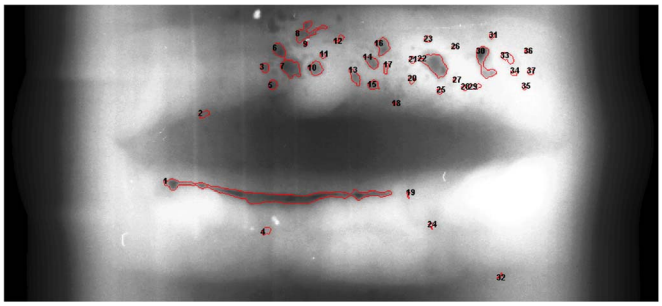

Fig. 8. Result of detection and labeling of discontinuities.

Table 1
Classes of defects in the database.

Defect classes	Samples
Porosity - PO	77
Slag Inclusion - SI	23
Lack of Fusion - LF	04
Crack - CR	08
No Defect - ND	146
TOTAL	258

Section 2.1. Fig. 8 shows the result for one of the images after the detection of discontinuities (potential defects). The edges of discontinuities found appear in red and the labels assigned by the labeling algorithm in black showing that 37 discontinuities were detected.

In the training step, a 9-dimension feature vector is generated for each detected descontinuity. The detected discontinuities are classified into five different classes (porosity, slag inclusion, lack of fusion, cracks and no defect) resulting in an unbalanced training set with 258 vectors and five output classes. Table 1 shows the defect classes and the number of available samples of each of them.

The database defined in Table 1 is used for training the MLP. Ten trainings were performed with different weight initializations and the result of the best training is presented in confusion matrix of Fig. 9. According to the confusion matrix, the overall accuracy for test data classification was equal to 79.5%. Results revealed a misclassification of the classes “lack of fusion”, “cracks” and “slag inclusion”. The best performance was achieved for class “porosity” followed by the “no defect” class with F-score of 81.48% and 85.10% respectively. The low performance of the classifier was mainly due to the unbalancing of the training set.

Taking into account the previous results, another simulation was carried out using only two classes: defect and no defect. All patterns of

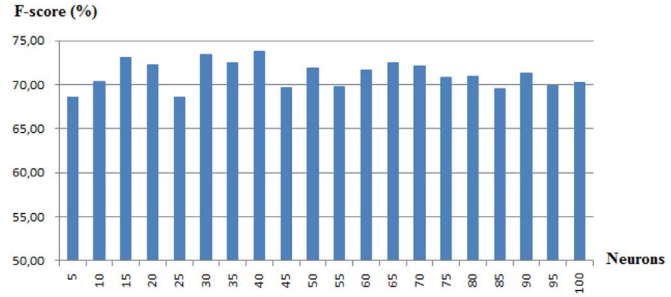

Fig. 10. Average F-score of the test data varying the number of neurons in the hidden layer.

defects listed in the previous experiment were grouped in the same class “defect” to provide a balanced training data set containing 112 vectors representing the class “defect” and 146 vectors representing the class “no defect”.

To determine the appropriate number of neurons in hidden layer 20 trainings were carried out for different number of neurons in the hidden layer. The number of neurons was varied from 5 to 100 with a regular increment of 5. Fig. 10 presents the average F-score of the test data for each set of trainings. Based on the results of these experiments, the optimum number of hidden neurons was chosen as 40, since more hidden neurons did not increase the F-score.

Using 40 neurons on the hidden layer the MLP was trained for classes: “defect” and “no defect”. The best result is presented in the confusion matrix in Fig. 11. The accuracy of the two classes was 88.6% with 87.5% F-score for the test data which shows an improvement over the previous classification of five classes.

Fig. 12 illustrates the stopping criterion described in Section 2.1.3. The training curve reveals that the validation error declines gradually and it was minimized at approximately 28 epochs. A total of 34 epochs was used. The overtraining occurs after 28 epochs, which is marked by an increase in the validation error.

The trained neural network with 40 neurons in the hidden layer was applied to the descontinuities obtained in the detection of descontinuities step. Results of the proposed automated classifier algorithm of two classes (defect and not defect) can be seen in Fig. 13. The discontinuities classified as defects appear in yellow and the discontinuities classified as no defect in red. In the Fig. 13 was placed the image classified by an expert for purposes of comparison to the results of the proposed algorithm. The approach presented in this paper does not deal with Tungsten Inclusion (TI) defect that appears in report of inspection showed in Fig. 13 since its characteristics are quite different from those investigated in the proposed approach. For this image only

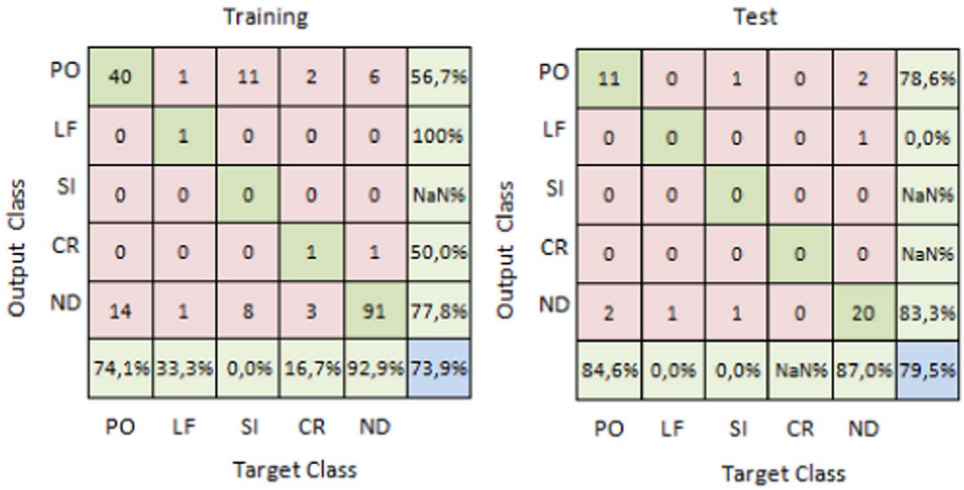

Fig. 9. Matrix confusion of a neural network training with 10 neurons in the hidden layer in the classification of 5 types of defects.

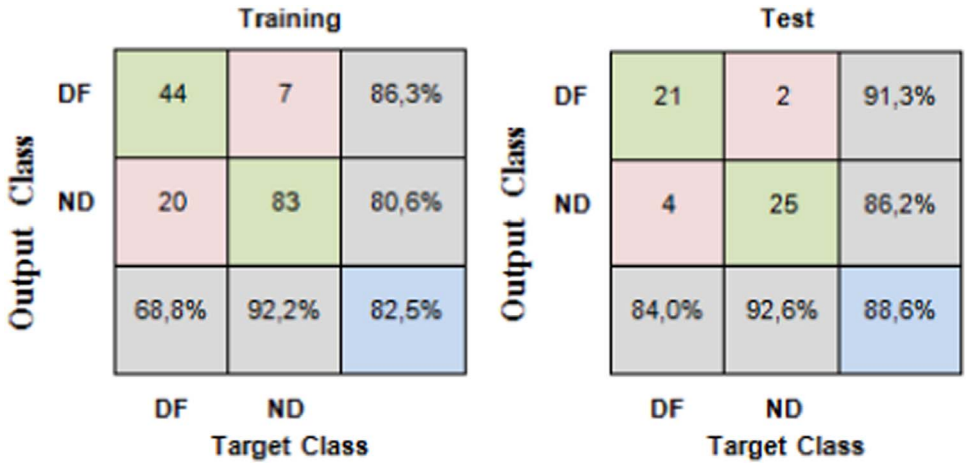

Fig. 11. Confusion matrix of a training of the MLP network with 40 neurons in the hidden layer to the classes defect and no defect.

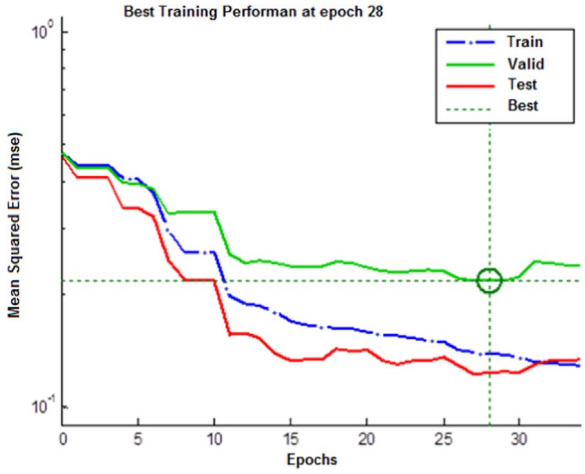

Fig. 12. Stopping criterion for training.

a discontinuity could not be correctly classified.

4. Conclusion

Radiography is a method for NDT widely used for testing pipelines welding. A large number of radiographic images are analysed by inspectors which can lead to a subjective interpretation with the potential risk of overlooking defects. Many efforts have been done towards the design and construction of automatic inspection systems, aiming at supporting the weld joint radiographs interpretation and, therefore, improving robustness, accuracy, and speed of the inspection process. Despite the large number of research publications on this issue there are few studies investigating automatic inspection of DWDI radiographic images, especially in real field.

In this research, an algorithm for automated detection of flaws in welded joints of petroleum pipelines has been developed using image processing techniques and a neural network. The basic idea is to try to mimic the way a human inspector would inspect radioscopic images: first the weld bead is located, followed by detecting descontinuities (potential defects) in the weld bead region and then such discontinuities are classified as defect or no-defect. A set of geometrical features is extracted from the detected descontinuities to be used as input to an MLP classifier. The experiments were performed on DWDI real field radiographic images which, usually, have a lower quality than the images used in other studies.

The attempt to perform the classification of defects was not successfully because there were few samples of each defect type generating a set of unbalanced data which led to misclassification of the descontinuities. In contrast, classification of the samples in two classes (defect and no defect) reached an F-score of 87.5% for the test data. It was observed that the number of hidden neurons in the MLP influences the network performance. The choice of this parameter was based upon a trial and error procedure.

This work aims to contribute towards an improvement of the automatic detection of welding defects in DWDI radiographic images. Despite the subjectivity involved in the evaluation of different methods, a comparison of the results with the earlier studies of authors who have

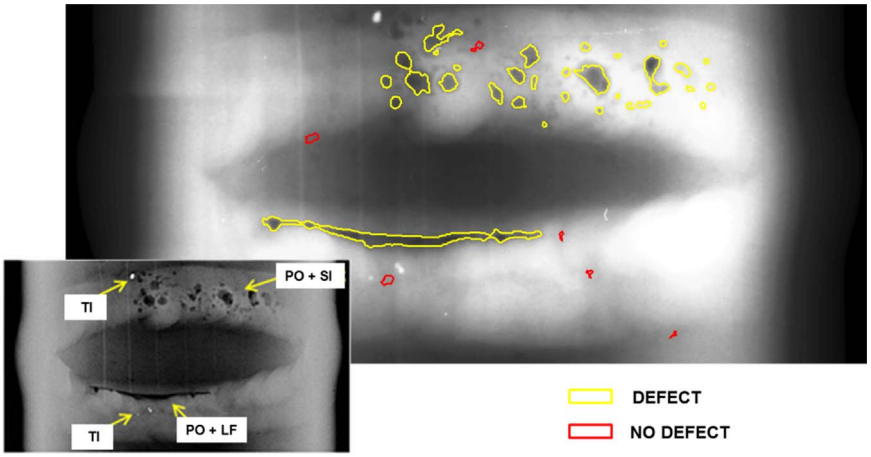

Fig. 13. Image after the automatic classification of discontinuities: in bottom plan – report of inspection provided by an expert.

used SWSI and DWSI radiographic images indicates that the proposed method is promising.

The application of the method in welding defect classification is work for future research. However, the determination of a set of attributes with a balanced representation of samples of each defect type, taking in account the specificities of the defects, requires further research to make a more accurate classification. Other strategies may be used to try to improve our results, such as, increasing the number of samples, use of texture features from defects, experiments with different neural network configurations and alternative learning algorithms.

References

[1] Quinn RA, Sigl CC. Radiography in modern industry, 4th ed.. Rochester, New York: Eastman Kodak Company; 1980.

[2] Godoi WC, da Silva RR, Swinka-Filho V. Pattern recognition in the automatic inspection of flaws in polymeric insulators. Insight-Non-Destr Test Cond Monit 2005;47(10):608–14.

[3] Lashkia V. Defect detection in X-ray images using fuzzy reasoning. Image Vis Comput 2001;v. 19:261–9.

[4] da Silva RR, Siqueira MHS, Calôba LP, Rebello JM. Radiographics pattern recognition of welding defects using linear classifiers. Insight 2001;43(10):669–74.

[5] da Silva RR, Calôba LP, Siqueira MHS, Sagrilo LVS, Rebello JMA. Evaluation of the relevant characteristic parameters of welding defects and probability of correct classification using linear classifiers. Insight 2002;44(10):616–22.

[6] da Silva RR, Calôba LP, Siqueira MH, Rebello JM. Pattern Recognit Weld Defects Detect Radiogr Test NDT E Int 2004;37(6):461–70.

[7] da Silva RR, SiqueiraMH , de Souza MPV, Rebello JM, Calôba LP. Estimated accuracy of classification of defects detected in welded joints by radiographic tests. NDT E Int 2005;38(5):335–43.

[8] Wang G, Liao TW. Automatic identification of different types of welding defects in radiographic images. NDT E Int 2002;35(8):519–28.

[9] Liao TW. Classification of weld flaws with imbalanced class data. Expert Syst Appl 2008;v. 35:1041–52.

[10] Liao TW. Improving the accuracy of computer-aided radiographic weld inspection by feature selection. NDT E Int 2009;v. 42:229–39.

[11] Valavanis I, Kosmopoulos D. Multiclass defect detection and classification in weld radiographic images using geometric and texture features. Expert Syst Appl 2010;37(12):7606–14.

[12] Shafeek HI, Gadelmawla ES, Abdel-Shafy AA, Elewa IM. Automatic inspection of gas pipeline welding defects using an expert vision system. NDT E Int 2004;37(4):301–7.

[13] Mirapeix J, García-Allende PB, Cobo A, Conde OM, López-Higuera JM. Real-time arc-welding defect detection and classification with principal component analysis and artificial neural networks. NDT E Int 2007;40(4):315–23.

[14] Vilar R, Zapata J, Ruiz R. An automatic system of classification of weld defects in radiographic images. NDT E Int 2009;42(5):467–76.

[15] Zapata J, Vilar R, Ruiz R. Performance evaluation of an automatic inspection system of weld defects in radiographic images based on neuro-classifiers. Expert Syst Appl 2011;38:8812–24.

[16] Balakrishnan R. Innovative RT Technique to Evaluate Flaws Location and Sensitivity in Tube Butt Welds in DWDI Technique. In: Proceedings of the National Seminar & Exhibition on Non-Destructive Evaluation, India; 2009.

[17] Edalati K, Rokrok B, Kermani A, Seiedi M, Movafegh A, Shahandeh M. Scattering and image contrast simulation for double wall radiography of pipes. Int J Press Vessels Pip 2007;84(7):441–50.

[18] Edalati K, Rokrok B, Kermani A, Seiedi M, Movafeghi A, Rastkhah N. Sensitivity evaluation in double wall radiography of pipes and multilayer plates by assessment the Monte Carlo simulation. J Test Eval 2006;34(6):562.

[19] Sang-Ki Park, Yeon-Shik Ahn, Doo-Song Gil. The Study on Evaluation for Digital Radiography Image of Weldments. In: Proceedings of the 10 International symposium of measurement technology and intelligent instruments ISMTII, Korea; 2011 p. 1–4.

[20] Kroetz M, Centeno TM, Delgado MR, Felisberto M, Lucas LA, Dorini LB, Fylyk V, Vieira A. Genetic algorithms to automatic weld bead detection in double wall double image digital radiographs. In: WCCI 2012 IEEE world congress on computational intelligenceintelligence, Brisbane; 2012.

[21] Suyama FM, Krefer AG, Faria AR, Centeno TM. Detecting Central Region in Weld Beads of DWDI Radiographic Images Using PSO. Int J Nat Comput Res 2015;5:42–56.

[22] Solomon CJ, Breckon TP. Fundamentals of digital image processing: a practical approach with examples in Matlab. Wiley-Blackwell; 2010.

[23] Gonzalez RC, Woods RE. Digital image processing. Pearson Prentice Hall; 2008.

[24] Otsu N. A threshold selection method from grey-level histograms. IEEE Trans Syst, Man Cybern 1979;9(1):41–7.

[25] Gonzalez RC, Woods RE, Eddins SL. Digital image processing using MATLAB. New York: Pearson Education; 2004.

[26] Sae-Tang S, Chularat T Feature windowing-based Thai text-dependent speaker identification using MLP with backpropagation algorithm. Proceedings. ISCAS 2000 Geneva. In: Proceedings of the 2000 IEEE International Symposium on Circuits and Systems. vol. 3. IEEE; 2000.

[27] Møller MF. A scaled conjugate gradient algorithm for fast supervised learning. Neural Netw 1993;6:525–33.

[28] Beale MH, Hagan MT, Demuth HB. Neural Network Toolbox™ 7. user's guide. accessed: 02/06/. available in: ⟨http://www.mathworks.com/help/pdf_doc/nnet/nnet_ug.pdf⟩; 2014.

[29] Sokolova M, Lapalme G. A systematic analysis of performance measures for classification tasks. Inf Process Manag 2009;v. 45:427–37.

[30] Fawcett T. An introduction to ROC analysis. Pattern Recognit Lett 2006;27(8):861–74.

[31] Powers D/MW. Evaluation: from precision, recall and F-measure to ROC, informedness, markedness & correlation. J. Mach. Learn. Technol. 2011;2(1):37–63.

Prof. Neury Boaretto received the B.S. degree in Electrical Engineering from State University of Santa Catarina – UDESC (1988), the M.S. degree in Production Engineering from Federal University of Technology - Paraná (2005) and he is doctoral student in Electrical Engineering and Computer Science from Federal University of Technology - Paraná. He was a member of the Department of Electronics of the Federal University of Technology - Paraná from 1993 until 2006. He is a member of the Department of Electronics of the Federal Institute of Santa Catarina - IFSC since 2007. His main interests are Computer Vision, Pattern Recognition, Digital Image Processing, Flexible Manufacturing Systems and Supervisory Systems.

Prof. Tania Mezzadri Centeno received the B.S. degree in Computer Science in 1985, the M.S. degree in Electrical and Computer Engineering from Federal University of Technology - Paraná (1994) and the Ph.D. in Computer Science from Université Paul Sabatier de Toulouse II (1998). She is a member of the Department of Informatics of the Federal University of Technology - Paraná since 1991 and has a Research Fellowship from National Council for Scientific and Technological Development (CNPq). She has received financial support for research projects from a number of funding agencies. Her main interests are Computer Vision, Pattern Recognition and Digital Image Processing.